Renewable and Sustainable Energy Reviews 30 (2014) 324–336

Contents lists available at ScienceDirect

Renewable and Sustainable Energy Reviews

journal homepage: www.elsevier.com/locate/rser

Effect of thermal annealing on P3HT:PCBM bulk-heterojunction organic solar cells: A critical review

Xiaohan Yang*, Ashraf Uddin

School of Photovoltaic and Renewable Energy Engineering, University of New South Wales, Sydney, NSW 2052, Australia

ARTICLE INFO

Article history:
Received 9 July 2013
Received in revised form
25 September 2013
Accepted 19 October 2013
Available online 9 November 2013

Keywords:
Organic solar cell
Thermal annealing
Physical film property
Electronic performance
Balancing

ABSTRACT

The main focus of this review article is to introduce the reader to the advantage and limitation of organic solar cells and to understand how the thermal annealing process could improve performance of organic solar cells. The article explores the operation principles of organic photovoltaic (OPV) device and reviews the effects of thermal annealing on bulk-heterojunction organic solar cells based on a thin film blend of poly (3-hexylthiophene-2,5 diyl) (P3HT) and [6,6]-phenyl-C_{61} butyric acid methyl ester (PCBM). It focuses on changes in the physical film properties, the electronic performance of devices, as well as the link between film structure and electronic performance during a thermal annealing process. Analysis of film and electrical characteristics, as a function of thermal annealing parameters, indicates that a balancing is established. The balancing between charge conduction and excitonic dissociation leads to the establishment of optimal annealing conditions for maximized electronic performance. Additionally, the report highlights research areas that require attention for future development of this technology.

Contents

* Corresponding author. Tel.: +61 2 9385 9827.
E-mail address: xiaohan.yang@unsw.edu.au (X. Yang).

1364-0321/$ - see front matter © 2013 Elsevier Ltd. All rights reserved.
http://dx.doi.org/10.1016/j.rser.2013.10.025

1. Introduction

Photovoltaic (PV) market is currently dominated by silicon solar cells, as silicon has excellent charge transport properties and is an abundant element on earth. Silicon solar cells have achieved a high power conversion efficiency (PCE) of 25% [1]. However, higher manufacturing costs, when compared to traditional power generation methods, have prevented PV from supplying a large portion of the stationary energy used in the world [2–4]. To further reduce the costs of current photovoltaic technologies, researchers have developed organic materials as possible candidates. The discovery of organic materials which have semiconductor properties has led to new field of organic light-emitting diode (OLED) [5] and OPV [6]. Solar cells based on organic materials can be fabricated using solution processing techniques, such as various coating, printing and roll to roll techniques, which could lower manufacturing costs by avoiding high temperature and vacuum processes [7–9]. Organic solar cells are lightweight and flexible, and can be fabricated on glass and plastic substrates [10,11]. The potential simplicity of OPV processing is far beyond other current technologies [12]. Furthermore, organic semiconductors have high absorption coefficients [13,14], which allow very thin films to be used. The last 5 years have seen significant progress for this technology [15–19]. To date, the highest reported PCE for an OPV device is 12% [20]. Considering the advantages and significantly increased efficiencies of OPV, it has resulted in commercial production of primary OPV products and a few public demonstration projects [21–23].

The progress of OPV has been accompanied with development of organic materials. Early work in OPV focused on a polymer, polyphenylene vinylene (PPV) as the donor material [24,25]. In 1995, Hummelen et al. synthesized one of the most important fullerene derivatives, PCBM, which represents a milestone in the development of OPV acceptors and is still widely used today [26]. After significant optimization, researchers achieved PCEs of more than 3% for PPV-based organic solar cells [27,28]. However, further improvement was limited by the relatively low hole mobility and narrow light absorption band [29], which led researchers to search for new donor materials. From 2002, P3HT with many advantages when compared to PPV, such as improved absorption and higher hole mobility [30], has become the favored polymer donor material. The organic system of P3HT:PCBM has been exposed to intensive research, in which the highest reported PCE values are in the range of 4.5 to 6% [31–33]. Due to the low excitonic diffusion length of organic semiconductors, typically ~10 nm [34–36], it is necessary to disperse the donor and acceptor phases intimately throughout the active layer. This produces an increased interfacial area, thus facilitating efficient excitonic dissociation. However, exciton dissociation is not the sole consideration for increasing electronic performance [29]. Efficient charge transport and extraction is dependent on the formation of percolated pathways within the photoactive layer. The physical arrangement of donor and acceptor phases in the active layer, referred to as the nanomorphology, is crucial in determining the electronic performance of an OPV device [25]. The nanomorphology of the blend is affected by several factors such as composition ratio of donor and acceptor, solvent materials, solution concentration, molecular weight and spin coating parameters [37–42]. Alternatively, control over the nanomorphology may be provided by preformed vertically aligned nanostructures, such as self-assembled P3HT nanowires [43,44] or vertically aligned metal oxide semiconductors [45–47]. To date, the most effective method for optimising the nanomorphology of the active layer is a thermal annealing process [48,49]. Multiple investigations into the effect of thermal annealing on OPV performance have been reported [50–54]. It has been suggested that the primary cause for increased PCE by thermal annealing, is an abrupt increase in hole mobility in the P3HT phase [29]. However, understanding the relation between the crystallinity and optical properties of the blended film, and the electronic performance of the OPV device is a pre-requisite for optimising the efficiency. Very few reports address this relationship in a comprehensive, systematic manner.

The first section of the review article outlines the concept of organic solar cells, detailing the device structure, operation principles and performance characteristics. In the second part, the effects of thermal annealing on P3HT:PCBM bulk-heterojunction organic solar cells are reviewed and a comprehensive list for optimal annealing conditions previously examined is presented. The significant finding in this report is a comprehensive description of the effect of annealing on both physical and electronic properties for a P3HT:PCBM bulk-heterojunction organic solar cell. A thorough analysis of the established balancing is provided in the discussion section. The balancing between charge conduction and excitonic dissociation leads to the establishment of optimal annealing conditions for maximized electronic performance. Such systematic studies of processing parameters are required to allow for up-scaling of production of organic solar cells. The conclusion provides a summary of effects of annealing on P3HT:PCBM organic solar cells. It also draws attention to important areas of research for the future.

2. Device structure and operation principles

2.1. Device structure

The device structure of organic solar cells is different from traditional silicon wafer based solar cells. The photoactive layer is a blend of conjugated polymers as electron donors and fullerene derivatives as electron acceptors. This photoactive layer is sandwiched between two electrodes with proper work functions. Fig. 1 shows a schematic diagram of conventional organic solar cell device structure. With this device structure, the light is illuminated through the glass substrate. The device is built on a transparent substrate which may be flexible. The substrates are usually glass or polyethylene terephthalate (PET). The anode consists of a semitransparent oxide layer, usually indium tin oxide (ITO). Its role is to allow light to pass through, and to collect holes from the device. A layer of the conductive polymer poly (3 4-ethylenedioxy-thiophene)-poly (styrenesulfonate) (PEDOT:PSS) is applied between the anode and the photoactive layer. This thin layer is spin coated on top of the ITO surface. The PEDOT:PSS layer serves as a hole conducting layer and exciton blocker. It smooths the ITO surface, seals the active layer from oxygen, and prevents the anode material from diffusing into the active layer, which can lead to trap sites [55]. The light absorbing photoactive layer containing the donor and acceptor material is sandwiched between two electrodes. For laboratory devices, this layer is spin coated from a common solution which contains the polymer donor and fullerene acceptor suspended in an appropriate solvent or mixture of solvents. The cathode is usually aluminium, although calcium or silver is sometimes used. The function

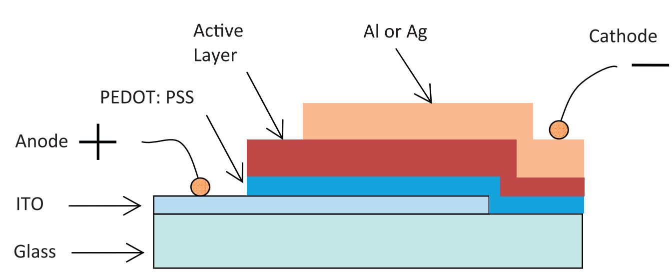


Fig. 1. Schematic diagram of organic solar cell device structure.

of the cathode is to collect electrons from the device. This layer is deposited by thermal evaporation.

2.2. Operation principles

As the fundamental properties of organic semiconductors are different to that of their inorganic counterparts, the operation of OPV devices is different to that of silicon solar cells. In a silicon solar cell, incident photons break the covalent bonds, which form electron–hole pairs. Due to the crystalline nature of silicon, generation of charge carriers requires only a small force of interaction. Therefore, absorption in silicon leads to effectively free charge carriers. As a result of the low dielectric constant ($\varepsilon \approx 3$) in semiconducting polymer materials, the columbic forces of attraction between electrons and holes are very high [49,56]. This implies that unlike inorganic semiconductors, in which photo excitation generally forms a free electron and hole, excited states in semiconducting polymers form bound electron–hole pairs. This bound electron–hole pair is referred to as an 'exciton'. A driving force is required to overcome this excitonic binding energy so that free charge carriers can be produced and transported throughout the device. In organic solar cells, excitons formed in the donor material can be dissociated at the donor–acceptor (D–A) interface. The force required to overcome the exciton binding energy is provided by the energy level offset of the lowest unoccupied molecular orbital (LUMO) of the donor and the LUMO of the acceptor material. Fig. 2 displays an energy band diagram of organic solar cells. This energy offset used to dissociate excitons is illustrated as ΔE_{ES} in Fig. 2, which is the excited state energy offset. In order to dissociate excitons formed in the acceptor material, the energy offset of the highest occupied molecular orbital (HOMO) of the acceptor and the HOMO of the donor material is required. This energy offset used to dissociate excitons is illustrated as ΔE_{GS} in Fig. 2, which is the ground state energy offset. Excitonic dissociation due to these energy offsets occurs at the interface between the donor and acceptor phase, therefore, the arrangement of the two materials in the active layer is crucial for the successful operation of the device.

Excitons can be created when photons are absorbed in the donor material. These excitons then can be dissociated at a D–A interface. Once separated, the electron can transfer to the acceptor material and be transported to the cathode for charge collection. The hole produced in the donor material travels throughout the polymer and is collected at the anode. This process is illustrated in Fig. 3(a). The fullerene acceptor material may also contribute useful photocurrent. When light is absorbed in the acceptor material, an exciton is formed which must be dissociated by the energy offset of the donor HOMO level and the acceptor HOMO level. The hole is then transferred to the donor at an interface and is transported to the anode whilst the electron remains in the acceptor material and travels to the cathode for collection. This process is demonstrated in Fig. 3(b).

The diffusion length of these bound electron hole pairs, or excitons is very small, in the order of 10 nm [34–36]. This causes very poor electronic response in organic devices fabricated using a bi-layer structure, similar to that of a p–n junction silicon solar cell, as only photons absorbed within a diffusion length of the junction can produce free charge carriers. A more successful approach is to disperse the donor and acceptor material intimately throughout the active region, which significantly increases the interfacial area. Such a design is referred to as a bulk-heterojunction device structure [25]. Fig. 4 displays a cross sectional illustration of both a bi-layer and BHJ device structure. A device with a large dispersion of interfaces throughout the photoactive layer requires smaller exciton diffusion distances, and thus, a larger exciton dissociation yield is achieved. There exists a trade-off between increasing interfacial area via the intimate dispersion of phases and the creation of efficient conductive pathways through which free electrons and holes may be transported. Therefore, the arrangement of donor and acceptor phase is thus crucial to device performance.

2.3. Performance characteristics

The power conversion efficiency of a solar cell is defined as:

$$PCE = \frac{J_{sc} \times V_{oc} \times FF}{P_{in}} \tag{1}$$

$$FF = \frac{J_m \times V_m}{J_{sc} \times V_{oc}} \tag{2}$$

where J_{sc} is short circuit current density, V_{oc} is open circuit voltage, FF is fill factor, P_{in} is incident input power, J_m and V_m are the maximum power point current density and voltage, respectively. To allow for valid comparison of device performance, an international standard for input power is used. This standard specifies an incident spectrum of AM 1.5 G, with an intensity of 100 mW/cm^2, whilst the cell is at a room temperature of 25 °C. Therefore, there are three major device characteristics which completely determine the efficiency of the device. Fig. 5 displays a typical illuminated J–V characteristic curve which illustrates these three characteristics.

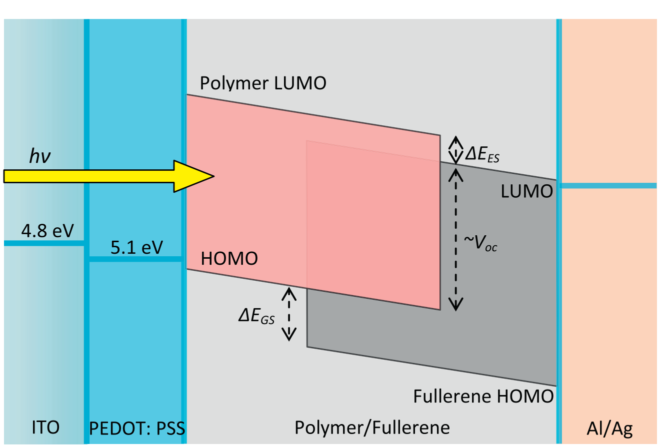


Fig. 2. Energy band diagram of donor–acceptor materials in bulk-heterojunction organic solar cells. Modified from [101].

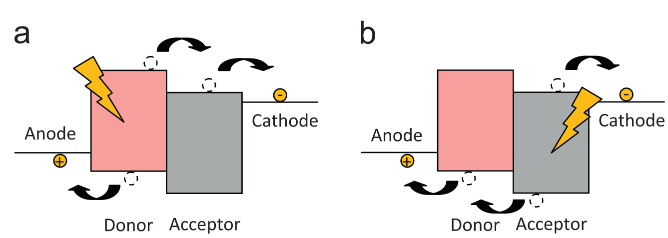


Fig. 3. Schematic energy band diagram displaying charge transfer for (a) photo generation in the donor, and (b) photo generation in the acceptor.

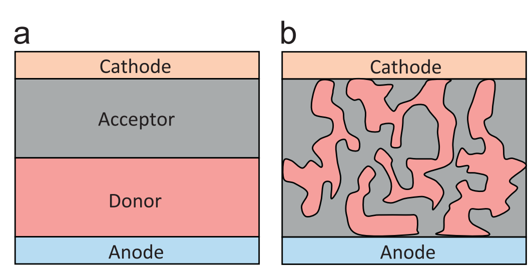


Fig. 4. Schematic diagrams of (a) bi-layer heterojunction and (b) bulk-heterojunction photoactive layers.

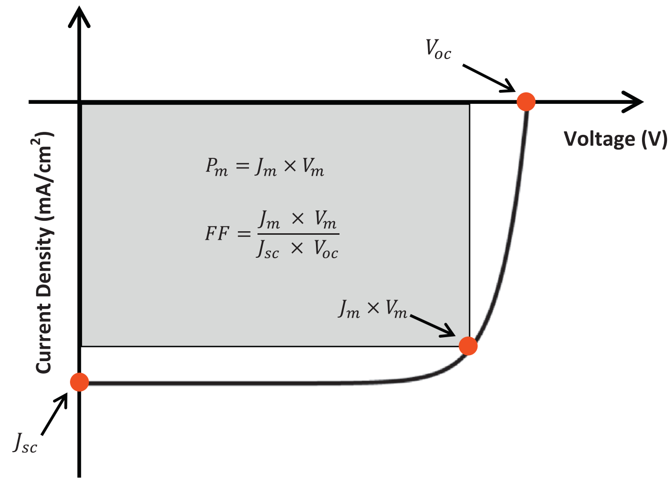


Fig. 5. *J*–*V* characteristics for a generic illuminated solar cell.

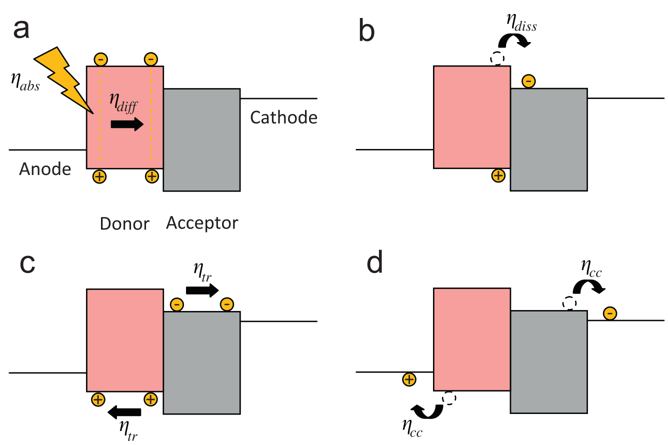


Fig. 6. The processes of photocurrent generation and transport. (a) Photon absorption and exciton diffusion, (b) exciton dissociation, (c) carrier transport and (d) charge collection. The efficiency of each one of these steps determines the EQE of the device.

The following describes the factors which influence these device characteristics for organic solar cells.

2.3.1. Short circuit current density

The short circuit current density (J_{sc}) is the maximum photocurrent density which can be extracted from the device at short circuit condition. The J_{sc} is directly related to the external quantum efficiency. This relationship can be expressed as:

$$J_{sc} = \frac{q}{\hbar c}\int_{\lambda_{min}}^{\lambda_{max}} EQE(\lambda) \times P_{in}(\lambda) \times d\lambda \quad (3)$$

where q is an electron charge, $\hbar$ is the Planck constant, c is the speed of light and λ is wavelength of the light. The EQE is the ratio of the number of charge carriers collected to the number of incident photons at a specific wavelength. For the operation of an organic solar cell, this quantity is dependent on five major steps, each of which has some associated efficiency. Therefore, EQE can be expressed as:

$$\text{EQE} = \eta_{abs} \times \eta_{diff} \times \eta_{diss} \times \eta_{tr} \times \eta_{cc} \quad (4)$$

The parameter η_{abs} describes the photon absorption efficiency of the device, which is illustrated in Fig. 6(a). Its improvement represents the most effective way of increasing the J_{sc} of an OPV device [57]. The absorption spectrum of the material is determined by both the band gap and absorption coefficient of the material, whilst the thickness of the active layer will also affect the absorption [58]. Additionally, thin film interference will affect the absorbance of the bulk-heterojunction photoactive layer. Current investigations using low band gap polymers are aimed at improving this characteristic [59–61]. In organic solar cells, significant useful absorption may be provided by the fullerene acceptor material as well, such as [6,6]-phenyl-C_{71} butyric acid methyl ester ($PC_{70}BM$). This implies that the electronic composition of the fullerene acceptor material will impact the J_{sc} of the device.

The parameter η_{diff} (Fig. 6(a)), describes the ability of an exciton to diffuse to a D–A interface. This is dependent on both the excitonic diffusion length, and the distance between excitons and the nearest interface, which is related to the nanoscale morphology of the photoactive layer. As the excitonic diffusion length in conjugated polymers is very low [34–36], control over the D–A arrangement is crucial for successful exciton diffusion. This factor is inversely related to the rate of recombination within the photoactive layer.

The exciton dissociation efficiency (η_{diss}) is demonstrated in Fig. 6(b). As the electron is still bound within the exciton, the energy offset formed at the D–A interfaces is required to provide a driving force which releases the electron and allows conduction to occur. This energy offset must be larger than the excitonic binding energy in the material to facilitate charge transfer. This energy is typically in the range of 0.1–0.5 eV [35,62]. This occurs only at the boundaries between the two materials, and thus, the distribution of the interface throughout the active layer is extremely important for the efficiency of the solar cell.

The efficiency of charge carrier transport throughout the device (η_{tr}) is displayed in Fig. 6(c). In organic materials, charge transport occurs via a process of hopping between energy states and is affected by traps and recombination sites in the photoactive film. The success of this transport depends greatly on the mobility of the associated organic materials [29].

The parameter η_{cc} describes the efficiency of charge collection at the electrodes. This represents the ability of the charge carriers to be injected into the electrodes from the photoactive layer, which is displayed schematically in Fig. 6(d). The success of this step is greatly dependent on the electronic composition of the device. For successful injection of electrons into the cathode, the magnitude of the LUMO level of the acceptor material, with respect to the vacuum level, must be lower than the work function of the metal. For successful injection of holes into the anode, the magnitude of the HOMO level of donor material, with respect to vacuum level, must be higher than the work function of the transparent anode. The material used for the electrodes must be carefully selected. A discrepancy between the work function of the anode and cathode material is required to provide a direction for the photocurrent. Usually intermediate layers between the photoactive layer and electrodes are introduced to make the injection of charge carriers more favorable [63,64]. The quality of the ohmic contact with the cathode, which is determined by the nature of the interface with the metal cathode, also affects the charge collection efficiency.

2.3.2. Open circuit voltage

Open circuit voltage (V_{oc}) is the difference of electrical potential between two terminals when a device is disconnected from any circuit. In contrast to silicon p–n junction solar cells, the origin of open circuit voltage in bulk-heterojunction devices is still not well understood. Multiple reports have investigated this property for OPV devices, using PCBM as the electron acceptor. In 2001, Brabec et al. [65] proposed an effective band gap model for bulk-heterojunction cells, whereby the maximal value of V_{oc} is related directly to the energy difference between the HOMO level of the

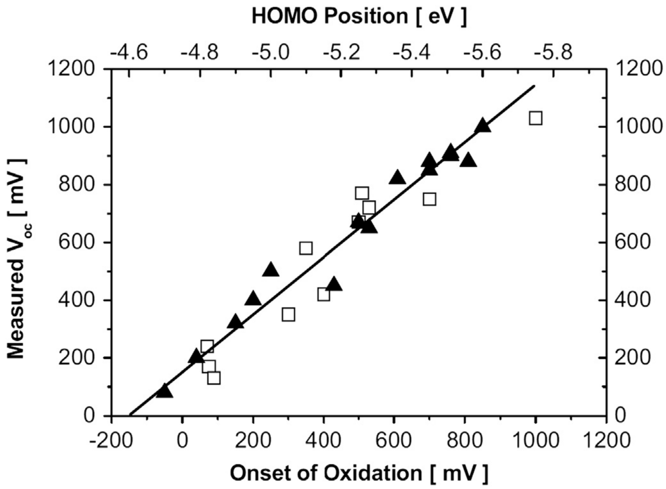


Fig. 7. V_{oc} of different bulk-heterojunction solar cells plotted versus the oxidation potential/HOMO position of the donor polymer, where squares represent the conjugated polymers and triangles represent the polymer materials proprietary to Konarka [66].

donor and the LUMO level of the acceptor, as shown in Fig. 2. This proposition was verified by an empirical investigation of the effect of electron affinity of fullerene acceptor on open circuit voltage. A linear relationship between electron affinity of acceptor and open circuit voltage was discovered. This study also showed that V_{oc} is weakly dependent on the type of metal used as the cathode.

In 2006, Scharber et al. [66] published a breakthrough communication on the origin of open circuit voltage for OPV. This report studied the relationship between the energy levels of the D–A blend and the open circuit voltage for 26 different bulk-heterojunction devices, as shown in Fig. 7. For each device, the acceptor material used was PCBM, whilst the donor material was varied. It was found that there exists a linear relationship between the HOMO position, which is related to the diagonal band gap of the heterojunction, and the open circuit voltage. From this analysis, a simple relationship between the HOMO of the donor material and the V_{oc} of the device was derived, which was reported as [66]:

$$V_{oc} = (1/q)(|E^{Donor}\text{HOMO}| - |E^{PCBM}\text{LUMO}|) - 0.3\ V \quad (5)$$

This suggests that V_{oc} is directly proportional to the diagonal band gap of the heterojunction. However, there exists an empirical loss factor related to the bulk-heterojunction design. The systematic nature of this study made the proposition of the effective band gap model convincing, however, these results are derived purely from empirical evidence, rather than theoretical understanding. Recently, a contradictory report found no linear relationship between the diagonal band gap of the heterojunction and V_{oc} [67]. It was shown that diagonal band gap serves as an upper bound for V_{oc}. Such reports highlight the remaining ambiguity regarding the origin of V_{oc} in bulk-heterojunction OPV devices.

2.3.3. Fill factor

The fill factor (*FF*) is a key parameter in evaluating the performance of solar cells, which is determined by Eq. (2). Due to physical limitations on diode quality, the practical limit to fill factor is less than the ideal value of 1. The behavior of a real diode will deviate from the ideal, primarily as a result of recombination occurring at the junction. For organic solar cells, the junction is the D–A interface, which is distributed throughout the entire photoactive layer. Deviations from the ideal case, and thus the shape of the *J*–*V* curve, can be quantitatively characterised by the parasitic loss mechanisms of series and shunt resistance. Zero series resistance ($R_s=0$) is ideal, however, poor conductivity through the active layer and reduced charge carrier injection to the electrodes represents increased series resistance. Conversely, the ideal diode case demands infinite shunt resistance ($R_{sh}=\infty$). Reduction in R_{sh} is caused by imperfections within the photoactive layer or current leaks at the interface between layers in the device [68].

Crystalline inorganic solar cells can achieve very good diode quality. Solar cells fabricated using silicon, GaAs and InP have achieved fill factors in excess of 80% [69,70]. Bulk-heterojunction organic solar cells generally display relatively lower fill factors. Non-ideal nanomorphology and discrepancy between electron and hole mobility are considered as main causes. Furthermore, the interface between active layer and cathode can play a important role in determining fill factor [71]. As the diode quality of a bulk-heterojunction device depends heavily on the nanomorphology and interfacial area of the photoactive layer, control over these components are crucial to restrain recombination and thus allow high fill factors to be achieved.

2.3.4. OPV efficiency limit

The power conversion efficiency is the most important performance parameter used to evaluate a solar cell, which is determined by Eq. (1). In 2009, Kirchartz et al. [72] implemented the theory of Shockley and Queisser to calculate radiative efficiency limits of bulk-heterojunction organic solar cells. For poly [9,9-didecanefluorene-alt-(bis-thienylene) ben-zothiadiazole] (PF10TBT) and PCBM blend cells, the radiative efficiencies are on the order of $\eta \approx 21\%$, however, current laboratory solar cells using the same materials achieve $\eta \approx 4\%$. Kirchartz et al. identified five loss mechanisms to explain this large gap between theory and experiment. These are (a) the difference between the energy of the exciton in the polymer and the charge transfer state at the D–A interface used in bulk-heterojunction solar cells leads to a small efficiency loss of 2%, while most losses are due to (b) optical losses caused by insufficient light trapping and parasitic absorption in layers that are not active in charge carrier collection, (c) losses caused by inefficient collection of photogenerated excitons, (d) recombination losses caused by a large amount of nonradiative recombination at the D–A interfaces or defects in the absorber, and (e) losses caused by relatively low charge carrier mobilities.

Kirchartz et al. [72] made a quantitative comparison of these loss mechanisms and found that the most dominant loss mechanism in organic solar cells is the nonradiative recombination at the D–A interface, by eliminating this factor, an increase in efficiency from 4.2% to 12.8% is achievable. Nonradiative recombination accounts for the loss in open circuit voltage, as well as for part of the loss due to carrier collection. Servaites et al. [73] also found that efficiencies of current bulk-heterojunction organic solar cells appear to be limited primarily as a consequence of incomplete exciton dissociation. In order to increase PCEs of OPV, it is critical to develop materials and improve D–A arrangement that enhance exciton dissociation and reduce nonradiative recombination.

Efficiency improvements can also be achieved by increasing the charge carrier mobility, therefore improving carrier collection and fill factor. An increase in exciton mobility will further enhance the photocurrent by increasing the amount of excitons to be dissociated. Additionally, due to the low refractive index of organic materials, comparatively small improvement may be obtained by introducing Lambertian light trapping schemes, hence novel light trapping techniques are needed to overcome the Lambertian limit [74].

3. Effects of annealing on P3HT:PCBM system

In a bulk-heterojunction design, there are two major performance considerations for the arrangement of donor and acceptor phases.

- Dispersion of donor and acceptor phase in the photoactive layer to allow for large interfacial area which leads to efficient excitonic dissociation.
- Establishment of continuous conducting pathways for good charge transport.

An as-cast P3HT:PCBM film is relatively amorphous in structure. This unordered structure severely limits the conduction and charge carrier mobility. As a result, non-annealed OPV devices often show low charge carrier mobility and ultimately low J_{sc} and fill factor. The purpose of an annealing step is to change the properties of the film from unordered and amorphous to a more homogenous nature. The film undergoes this transition as a result of an alignment of the polymer chains to form crystallites [75]. A schematic diagram depicting this transition is displayed in Fig. 8. For higher annealing temperatures, the PCBM phases diffuse and form aggregate. This aggregation can reduce successful excitonic dissociation. The thermal annealing parameters of both temperature and time vastly affect the rate at which this transition occurs and thus there exists some non-obvious optimum conditions which provide the most favourable excitonic dissociation and charge carrier conduction. This section will survey the changes induced by thermal annealing on the physical film structure and, as a result, the changes in device electronic performance.

3.1. Film characteristics

Physical changes which occur in the film as a result of the thermal annealing process will ultimately affect the device performance. It is important to understand how structural changes are linked to changes in electronic performance. The three most important film characteristics for an OPV blend are nanomorphology organisation, crystallinity and absorption profile. These three characteristics are discussed in detail in this section.

3.1.1. Nanomorphology organisation

The local nanoscale organisation of the donor and acceptor in the active layer has a profound impact on the PCE of the device. Intense study of the P3HT:PCBM system has led to an understanding that an annealing treatment induces a more stable nanoscale network with a higher degree of crystallinity and order. Traditionally this has been characterised using 2D microscopy analysis of atomic force microscopy (AFM) or transmission electron microscopy (TEM), however, this provides only ambiguous

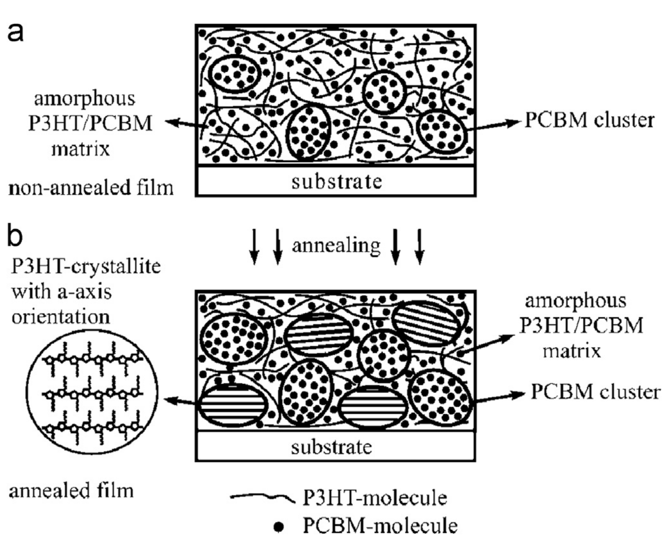


Fig. 8. Schematic pictures displaying the changes in the P3HT:PCBM blend film as a result of annealing [54].

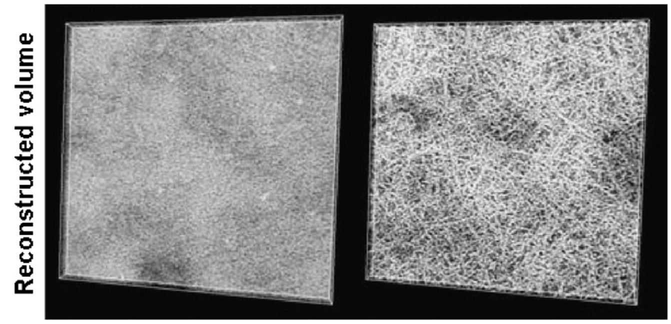


Fig. 9. Electron tomography images for P3HT:PCBM photoactive layers. The image on the left represents an as-cast film, whilst the image on the right is thermally annealed at 130 °C for 20 min [76].

evidence of a volumetric rearrangement and reordering. Recent attempts to provide a 3D visualisation have led to the adaptation of electron tomography for use in OPV. Bavel et al. [76] have utilised this technique to display the actual formation of crystalline 3D networks as a result of thermal annealing. This information is displayed in Fig. 9.

The 3D representation of the as-cast film shows that the formation of P3HT crystals is defective. This is contrasted in the annealed film, shown on the right, which displays the formation of a 3D nanoscale network. This volumetric representation shows how the physical film is altered as a result of thermal treatment.

3.1.2. Crystallinity

The crystallinity induced in the P3HT as a result of annealing is important for the facilitation of charge transport to the electrodes. This property of the material can be elucidated using x-ray diffraction (XRD), which measures a peak with some intensity and width for specific crystalline planes within a material. Although P3HT does not have a repeating crystalline structure like an inorganic semiconductor, e.g. silicon, it is still useful to analyse the structure of the regioregular chains as an analogue to crystallinity. An increase in intensity of a given peak indicates an increase in the size of the crystalline domains within the material. XRD spectra for a P3HT:PCBM film is displayed in Fig. 10. An increased intensity for the peak at 2 theta=5 degrees (corresponding to the inter-chain spacing in P3HT associated with the inter-digitated alkyl chains) [77], as a result of annealing shows a definite increase in crystallinity after an annealing step at 150 °C. This hypothesis is supported by multiple reports in literature [49,78,79].

3.1.3. Absorption spectra

The absorption profile of the active layer is very important as it will ultimately limit the maximum obtainable J_{sc}. The effect of annealing on the absorption profile is characterised with UV–vis spectroscopy. Two phenomena are generally observed as a result of thermal annealing. Both a red-shift in peak absorption and an increase in magnitude of absorption are observed for a P3HT:PCBM blend [80]. An absorption profile of an as-cast and annealed P3HT:PCBM is displayed in Fig. 11.

Analysis of the P3HT:PCBM films clearly display both of these traits. This will lead to an overall observable increase in useful absorption. With reference to the pure P3HT film, the absorption of the P3HT:PCBM film is blue-shifted and the vibronic structure of the as-cast P3HT is lost, due to the disruption of P3HT internal order as a result of PCBM addition. Upon thermal annealing, the absorption is red-shifted and the vibronic structure is restored. These changes are attributed to an increase in internal order, as the polymer chains are able to move more freely at higher temperatures. The magnitude of

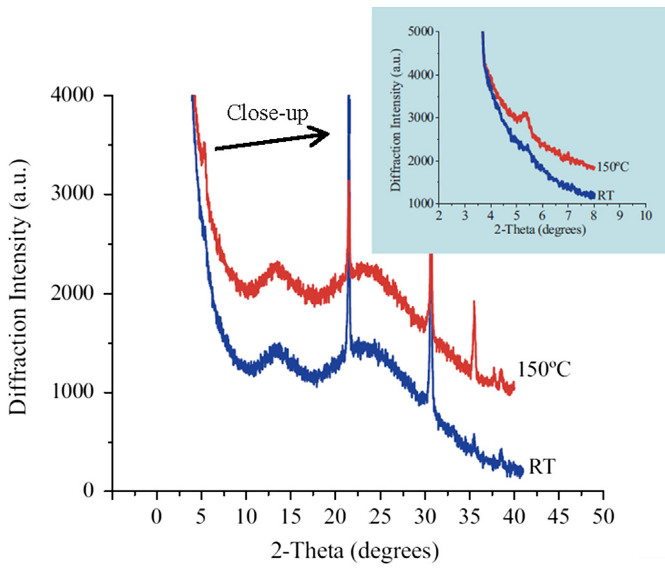


Fig. 10. Comparison of x-ray diffraction spectra of a P3HT:PCBM OPV device. This displays both non-annealed (blue) and thermally annealed at 150 °C for 30 min (red). The inset shows a close-up of the 2 theta values around 5 degrees [77]. (For interpretation of the references to color in this figure legend, the reader is referred to the web version of this article.)

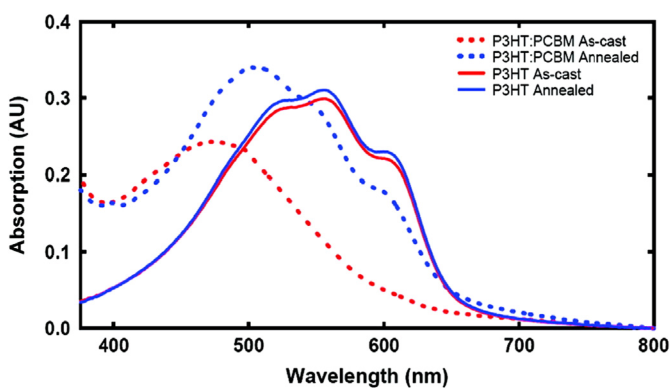


Fig. 11. UV–vis spectra for both pure P3HT and P3HT:PCBM blend films. Data for as-cast (red) and thermally annealed at 150 °C for 15 min (blue), is displayed [80]. (For interpretation of the references to color in this figure legend, the reader is referred to the web version of this article.)

absorption also increases, by 50%, which is a result of a higher degree of inter-chain interaction [80].

The process of thermal annealing causes P3HT to crystallise which induces a thermodynamically driven alteration of the photoactive layer. This causes a rearrangement of donor and acceptor phases, an increase in crystallinity of the P3HT and an improved absorption profile. These transformations lead to improvements in the electronic performance of the device, which will be discussed further in the following section.

3.2. Electronic characteristics

Alterations in device electronic performance can be characterised by current–voltage characteristic curves, EQE and mobility measurements.

3.2.1. Current–voltage measurements

It is common to compare the characteristics curves of devices subjected to different processing parameters to optimise performance. Ma et al. [77] have undertaken a comprehensive study of

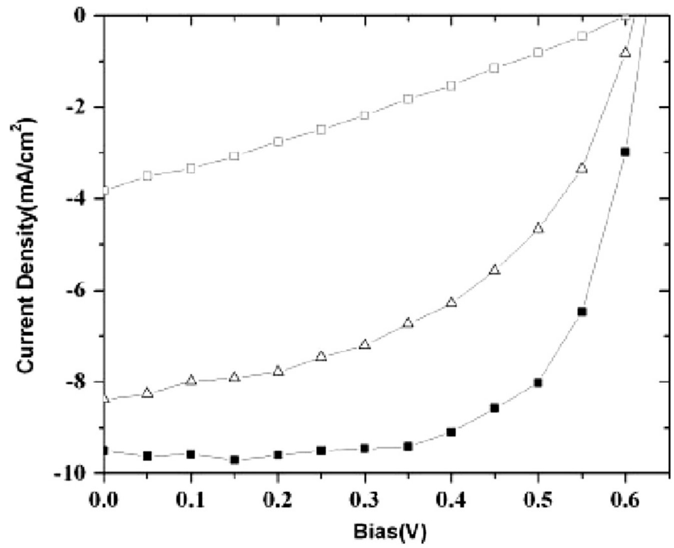


Fig. 12. Current–voltage characteristic curves of P3HT:PCBM solar cells with different treatments. Data is shown for three varying heat treatments of (i) no thermal annealing (open squares), (ii) thermal annealing at 70 °C (open triangles) and (iii) thermal annealing at 150 °C (filled squares). The illumination intensity used was 80 mW/cm^2 [77].

the process parameters of annealing temperature and time for a P3HT:PCBM system. A comparative study of *J–V* curves of devices with treated with different annealing temperature is displayed in Fig. 12.

It is evident from these *J–V* curves that thermal annealing leads to an improvement of electronic response. The annealing step leads to a marked increase in J_{sc} and a significant improvement in fill factor. The as-cast device displays poor device characteristics with J_{sc}=3.83 mA/cm^2 and FF=30%, as evidenced by the almost linear profile of the *J–V* curve. Thermal treatment with the intermediate temperature of 70 °C leads to an improvement in both of these characteristics, as it is believed crystallinity of the P3HT phase has begun to improve. Thermal treatment at 150 °C yields a distinct improvement in these two device characteristics. The J_{sc} increases to a value of 9.5 mA/cm^2, whilst the fill factor increases from 30% in the as-cast sample to 68% in the sample annealed at 150 °C. This vast improvement was linked to a reduction in series resistance. A quantitative comparison of series resistance was conducted by extracting the parameter from a modified ideal diode equation. The series resistance was seen to decrease by more than an order of magnitude (from 113 Ω cm^2 to 7.9 Ω cm^2) as a result of thermal annealing at 150 °C. These significant improvements are attributed to an optimisation of two crucial performance parameters, higher nanoscale crystallinity and an improved microstructure of demixed donor and acceptor phases.

3.2.2. External quantum efficiency measurements

The external quantum efficiency describes the amount of useful charge carriers produced for a certain amount of incident photons and is dependent upon the five major processes involved in organic solar cell operation. The J_{sc} of the device is directly linked to the EQE, shown in Eq. (3).

Yang et al. [30] have investigated the effect of annealing on P3HT:PCBM devices. Fig. 13 displays an EQE profile for pristine and annealed cells. The EQE response for the annealed sample is better for a wide spectral range. The authors note that enhanced current output is particularly present for the longer wavelengths. This increase in IPCE values lead to an enhancement in the magnitude

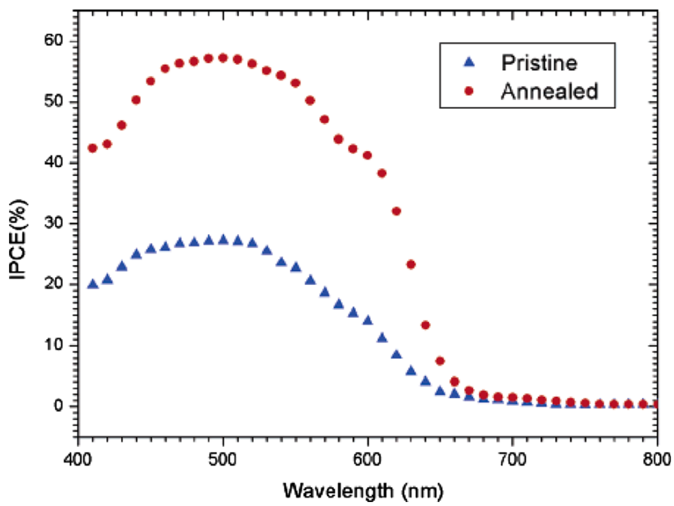


Fig. 13. External quantum efficiency profile for pristine (blue) and thermally annealed at 120 °C for 60 min (red) P3HT:PCBM devices [30]. (For interpretation of the references to color in this figure legend, the reader is referred to the web version of this article.)

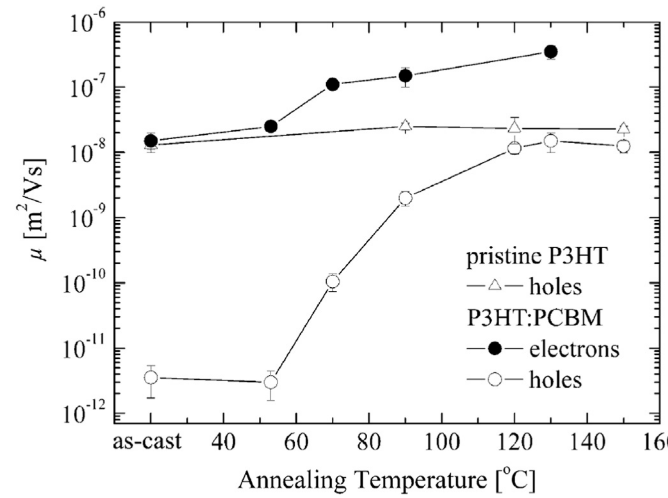


Fig. 14. Calculated zero-field mobilities of electrons (filled circles) and holes (open circles) for P3HT:PCBM devices as a function of annealing temperature. As a reference, the calculated zero-field mobility of holes (open triangles) in pristine P3HT is also displayed [29].

of J_{sc} from 3.1 mA/cm^2 to 7.4 mA/cm^2. This increase is consistent with the results obtained by Ma et al. [77]. The enhanced device performance is attributed to the formation of thin fibrillar crystals of P3HT which induce a crystalline order in the blend. This is evidenced by bright field TEM analysis. It is believed that this fibrillar crystalline structure leads to enhanced charge transport which causes the higher EQE and J_{sc} values. Quantitative electronic characterisation of charge transport can be obtained by measuring the mobility of the donor and acceptor material within the blend.

3.2.3. Mobility

It is important to quantify the change in charge carrier transport properties as a result of a thermal annealing step. Mihailetchi et al. [29] achieved this by determining the hole and electron mobility of a P3HT:PCBM device as a function of varying annealing temperature. The most important factor which affects J_{sc} is the magnitude of the hole mobility. For pristine devices, the J_{sc} is fundamentally limited by a discrepancy between hole and electron mobility which leads to a build-up of space charge. For a P3HT:PCBM blend, the electron mobility of the acceptor is much higher than the hole mobility, causing a bottleneck of charge carriers. It is thus important to understand how the magnitude of mobility values change due to annealing, as well as understanding the discrepancy between hole and electron mobility.

There are multiple measurement systems to quantitatively analyse mobility which include field effect transistors (FET), time of flight (TOF) photocurrent measurements and space charge limited (SCL) current measurements. Different magnitudes of charge carrier mobility have been reported due to different measurement techniques. The value of mobility also depends on the molecular weight of P3HT, concentration ratio between P3HT and PCBM in the blend and annealing temperature.

The authors use a method to determine electron and hole mobility from current-voltage measurements, which utilises the same set up and experimental conditions as used for the operation of a solar cell. By varying the work function of the electrodes, the injection of either electrons or holes may be quenched. This will result in the formation of either hole- or electron-only devices, respectively. For hole- or electron-only devices, the space charge limited current is approximated by the following formula:

$$J_{e(h)} = \frac{9}{8}\varepsilon_0\varepsilon_r\mu_{e(h)}\exp\left(0.891\gamma_{e(h)}\sqrt{\frac{V}{L}}\right)\frac{V^2}{L^3} \qquad (6)$$

where $J_{e(h)}$ is electron (hole) current, $\mu_{e(h)}$ is zero-field mobility of electron (hole), $\gamma_{e(h)}$ is field activation factor, ε_0 is permittivity of free space, ε_r is relative permittivity of the material, V is applied voltage and L is thickness of the active layer.

Fig. 14 displays the zero-field mobilities for holes and electrons as a function of annealing temperature, calculated from Eq. (6). This figure shows that the hole mobility of P3HT is significantly reduced as a result of introducing PCBM in a blend, with reference to the mobility in pristine P3HT. This is attributed to the disruption of the crystalline nature of the P3HT by adding PCBM molecules. It is believed that the process of annealing allows the crystallisation of P3HT and a demixing of the two phases. This leads to the formation of an interpenetrating network consisting of P3HT crystals and aggregated PCBM nano crystallites which lead to the formation of efficient conducting pathways which provide improved electron and hole mobilities [29]. The figure also suggests that the rapid increase in hole mobility as a function of annealing temperature leads to a better balance between electron and hole mobility values, which reduces the build-up of undesirable space charge.

Analysis of the thermally induced changes in electronic performance leads to the conclusion that the process of thermal annealing improves the performance of OPV devices. This is caused by the increasing trends of both fill factor and J_{sc}, whilst V_{oc} remains relatively constant for all temperatures. This improvement occurs as some optimisation is reached between properties of charge transport and excitonic dissociation, as a result of crystallinity induced in the polymer and a more favourable arrangement of the donor and acceptor phases. The balancing implies that there exists some optimum annealing temperature for P3HT:PCBM OPV devices. Ma et al. [77] have suggested that this optimum occurs using the processing conditions of 150 °C for 30 min. The authors produced a comprehensive study of efficiency as a function of annealing temperature to draw this conclusion. This study is displayed in Fig. 15. Increasing annealing temperature leads to improved efficiency, due mainly to improvements in charge transport properties. This improvement ceases at 150 °C, where an optimum point is found. A reduction in efficiency for annealing temperatures higher than 150 °C is observed. Temperatures in this range lead to the aggregation of the PCBM molecules, which results in a decrease in interfacial area. This leads to a reduction in the excitonic dissociation efficiency for these temperatures which is the cause of the reduction in PCE. Other authors have reported similar observations for optimal annealing conditions. Table 1 displays a non-exhaustive

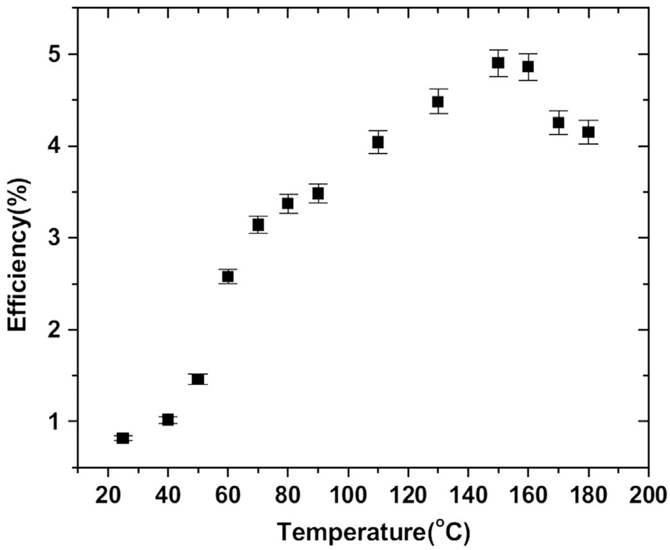


Fig. 15. Power conversion efficiency versus thermal annealing temperature for P3HT:PCBM devices, with a constant annealing time of 15 min [77].

Table 1
Thermal annealing parameters and device performance data for organic solar cells as reported in literature. The materials used in the active layer were P3HT:PCBM.

Solvent	Temp (°C)	Time	J_{sc} (mA/cm²)	V_{oc} (V)	FF	PCE (%)	Illumination	Ref
CB	158	8 min	15.4	0.66	0.6	6.1	1 sun	[33]
CB	150	30 min	9.5	0.63	0.68	5	0.8 suns	[77]
CB	155	5 min	11.1	0.65	0.54	4.9	0.8 suns	[81]
CB	140	2 h	11.5	0.62	0.52	4.4	0.85 suns	[53]
CB	155	5 min	9.61	0.56	0.6	4.3	0.76 suns	[82]
CB	150	10 min	9.77	0.66	0.623	4.02	1 sun	[83]
CB	150	30 min	8.93	0.60	0.629	3.4	1 sun	[84]
CB	130	10 min	9.48	0.64	0.56	3.39	1 sun	[85]
CB	130	10 min	5.16	0.57	0.538	3.16	0.5 suns	[86]
CB	120	60 min	10.3	0.65	0.47	3.1	1 sun	[87]
CB	140	15 min	9.4	0.61	0.55	3	1 sun	[51]
CB	140	10 min	7.328	0.617	0.567	2.57	1 sun	[88]
CB	110	10 min	6.8	0.58	0.42	1.7	1 sun	[78]
CB/NtB	150	15 min	10.5	0.66	0.62	4.3	1 sun	[32]
Chloroform	130	20 sec	–	–	–	3.6	0.5 suns	[54]
Chloroform	120	4 min	–	–	–	2.85	1.15 suns	[29]
Chloroform	130	20 sec	6.35	0.6	0.632	2.39	1 sun	[50]
DCB	130	30 min	14.1	0.65	0.6	5.5	1 sun	[31]
DCB	110	10 min	10.6	0.61	0.674	4.37	1 sun	[52]
DCB	160	10 min	10.55	0.664	0.61	4.26	1 sun	[89]
DCB	150	10 min	11.62	0.57	0.58	3.84	1 sun	[90]
DCB	75	4 min	8.5	0.55	0.6	3.5	0.8 suns	[91]
DCB	175	10 min	9.25	0.62	0.588	3.38	1 sun	[92]
DCB	140	10 min	9.2	0.68	0.37	2.32	1 sun	[93]
ODCB	130	20 min	10.9	0.58	0.61	3.8	1 sun	[76]
ODCB	120	60 min	7.2	0.615	0.61	2.7	1 sun	[30]
Toluene	150	15 min	8.3	0.56	0.62	3	1 sun	[80]

list of observed optimal annealing process parameters as inferred from literature.

3.3. Link between film structure and electronic performance

The process of thermal annealing has an impact on both the physical nature of the film and thus the electronic performance of the device. For efficient optimisation of OPV devices, it is crucial to understand the link between these properties. This is vitally important in the current context of exploration of low band gap polymers, with differing chemical properties, to replace P3HT. The traditional technique of AFM used for obtaining topographical data, coupled with *I–V* data can provide only ambiguous evidence of the structural–electronic relationship. New characterisation techniques, such as conductive atomic force microscopy (C-AFM), are required to improve our knowledge of the link between physical and electronic properties. C-AFM is a technique which measures surface topography and local electronic measurements simultaneously. It does this via a metal coated AFM probe which is connected to an external circuit [80]. The simultaneous measurement of these two properties provides a direct link between the arrangement of donor and acceptor phases and some electronic characteristics.

Dante et al. [80] utilised this technique to investigate the effect of annealing on P3HT:PCBM films. Fig. 16 displays cross sectional phase and hole current images of both non-annealed (a and c) and thermally annealed (b and d) P3HT:PCBM samples. This analysis shows that both an increase in the P3HT domain and the two domains are more uniformly distributed as a result of the thermal treatment. This correlates to an increase in the high current regions in the hole current image for the annealed sample. The authors concluded that improved device performance due to improved nanoscale ordering and increased charge carrier mobility. The ability for C-AFM to provide a direct link between nanomorphology and electronic performance makes it a viable tool for characterisation of multi component active layers.

3.4. Post vs. pre annealing

Another parameter associated with thermal annealing is the sequence in which it is performed, with respect to the metallisation step. Kim et al. [88] investigated the effect of the annealing sequence on both the film and electronic characteristics of P3HT:PCBM solar cells. The current–voltage characteristics were investigated for four different device treatments, being (i) untreated, (ii) pre-annealed, in which the film was annealed prior to the aluminium metallisation, (iii) pre- and post-annealed, in which the films were annealed both before and after the aluminium metallisation and (iv) post-annealed, in which the films were annealed only after the metallisation step. This is displayed in Fig. 17.

This analysis shows that the post annealing step led to improved device performance, which was attributed to two factors. First, the post annealing step was deemed to increase the interfacial area between the aluminium cathode and the active layer. This improved contact lead to more efficient charge collection. Additionally, a slight increase in absorption was measured for the post annealed device, which was due to an increase in interfacial roughness between the active layer and aluminium. The performance of the post-annealed was better than both the untreated and pre-annealed device, which suggests that the sequence of the processing step is important, and that device post annealing is crucial in obtaining efficient charge carrier collection.

4. Discussions

It is found that there is a balancing between the optimum thermal annealing temperature and the electronic performance of P3HT:PCBM devices. Fig. 18 displays the features of the balancing with reference to changes in both the physical film and electronic performance. Annealing at low temperatures provides the molecules in the film with energy to move and re-arrange which has the effect of increasing crystallinity in the P3HT phase, as shown in Fig. 18(a)(i). This change in the physical film corresponds to an improvement in the electronic performance, due to improved conduction of charge carriers as shown in Fig. 18(b)(i). Annealing at higher temperatures, leads to the diffusion and aggregation of PCBM molecules, as shown in Fig. 18(a)(ii). This aggregation leads

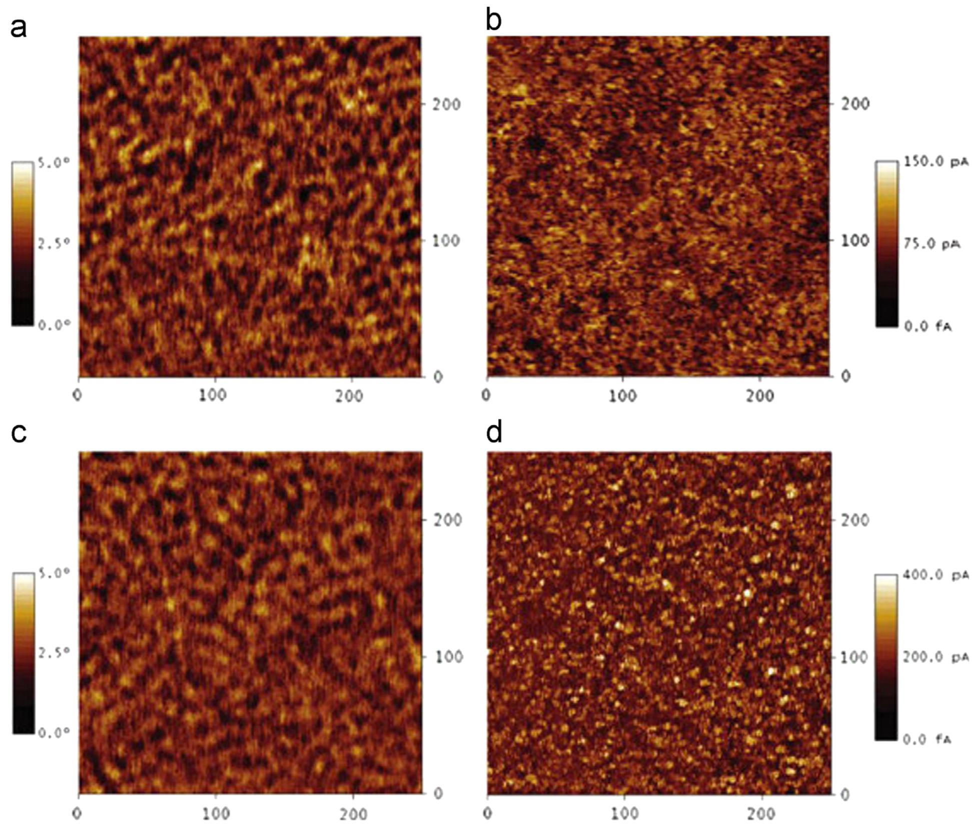


Fig. 16. Conductive AFM images for non-annealed ((a) and (b)) and annealed ((c) and (d)) P3HT:PCBM films. Images in the left column ((a) and (c)) show phase information while images in the right column ((b) and (d)) show hole current [80].

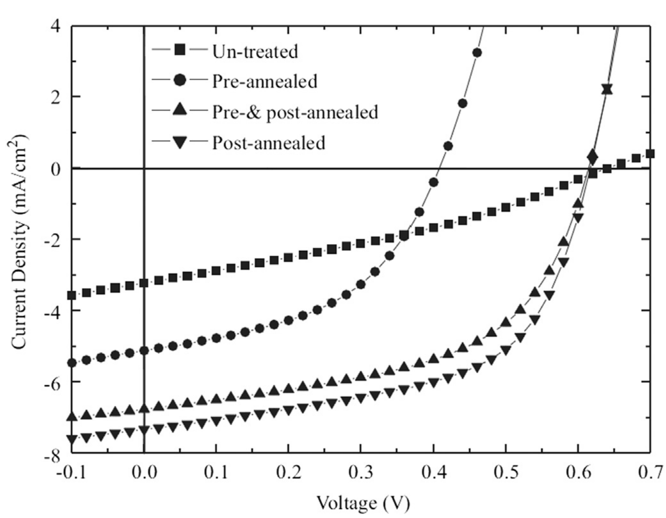


Fig. 17. Current–voltage characteristic curves for (i) untreated (squares), (ii) pre-annealed (circles), (iii) pre- and post-annealed (triangles up) and (iv) post-annealed (triangles down). The illumination intensity used was 100 mW/cm^2 [88].

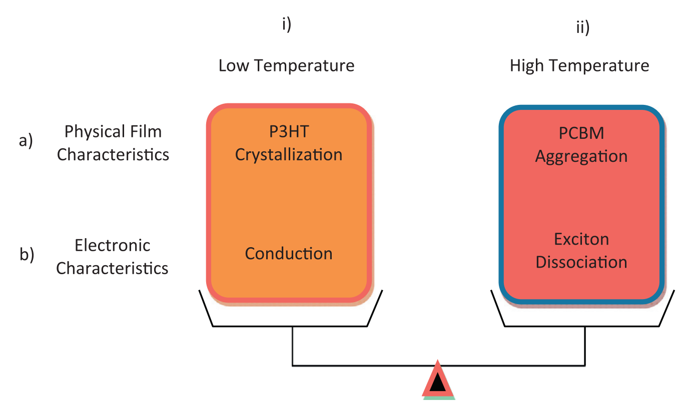


Fig. 18. Schematic drawing illustrating the nature of the balancing for the effect of thermal annealing on bulk-heterojunction organic solar cells.

to a reduction in the D–A interfacial area, which reduces the ability to dissociate excitons, as shown in Fig. 18(b)(ii). It has a negative impact on electronic performance. The balance between conduction and excitonic dissociation leads to the establishment of optimal annealing conditions for maximized electronic performance, as summarized in Table 1. The table suggests that the optimal annealing conditions for a P3HT:PCBM OPV device are variable from batch to batch, depends on the purity, polydispersity index (PDI) and molecular weight of P3HT. This study represents a systematic evaluation of thermal annealing condition for the material combination of P3HT:PCBM. To allow for large scale fabrication of OPV devices with optimized photoactive layers, further systematic studies of film processing parameters are required for P3HT:PCBM systems, as well as for films using new polymer materials.

To further advance the OPV technology, it is important to find the most appropriate combination of donor and acceptor materials used in organic solar cells. This requires careful consideration of the individual material band gaps, which affects the amount of absorption and thus the maximum obtainable J_{sc}, and the diagonal band gap of the heterojunction, which governs the maximum obtainable V_{oc}. Additionally, the ground state and excited state energy offsets, which determine the ability for

excitons to dissociate, need to be considered. Narrowing the band gap can improve J_{sc}, but V_{oc} may correspondingly be reduced due to the higher HOMO level that results. Moreover, other parameters such as carrier mobility, crystallinity and molecule chain packing also affect J_{sc}. Therefore, it is necessary to synthesize new low band gap polymers which can achieve improved J_{sc} and V_{oc} simultaneously.

Although steady progress has been achieved in improving PCEs of organic solar cells, the short device lifetime has remained a liability and limited the progress of OPV commercialization. It has been found that using fullerenes as the electron acceptor in bulk-heterojunction organic solar cells induces instability in the photoactive layer [94]. PCBM tends to aggregate as a consequence of elevated temperatures, even after time at room temperature. To improve the cell stability, PCBM can be replaced by more stable acceptor or using polymers with high glass transition temperature [95]. Additionally, oxygen, water and continuous illumination have been shown to cause device degradation [94,96]. Schumann et al. [97] have demonstrated an improvement in stability of inverted P3HT:PCBM devices by replacing PEDOT:PSS with a ZnO layer. The overall decrease in PCE for a device with ZnO layer is 19.3% after 40 h continuous illumination at 100 mW/cm^2, when compared to 60.3% for a device without ZnO. The improvement in device stability is related to a reduced oxidation of the polymer, as oxygen and water are blocked by the ZnO layer. The device stability has a significant impact on progress of OPV, more works need to be done such as modifications to the traditional cell structure.

Many research groups have reported high efficiencies OPV for small area devices using laboratory processing methods, for instance, spin coating and thermal evaporation. The next step for this promising field is to produce large area solar modules using high output, low cost fabrication techniques. Although there are a few demonstrations on roll to roll processing techniques [98–100], this is still a challenge as many processing parameters used for laboratory scale device production, are not directly transferable to large scale production. More effort must be directed on optimizing processing parameters, particularly for layers coating within device fabrication.

5. Conclusion

The effect of thermal annealing on P3HT:PCBM bulk-heterojunction organic solar cells is reviewed. Thermal annealing was seen to improve the absorption of the film, due to the formation of a more ordered polymer structure. The crystallinity of the polymer phase was greatly enhanced due to thermal annealing, as evidenced by XRD. This induced change in film properties was linked to a change in electronic characteristics of the OPV device. Thermal annealing temperatures up to the optimal value led to an improvement in performance. However, annealing temperatures higher than this value caused a reduction in electronic performance. It was found that a balancing governs the optimum thermal annealing temperature for a bulk-heterojunction device. Low annealing temperatures induce crystallinity in the polymer phase which leads to an improvement in charge carrier conduction. However, thermal annealing temperatures above the optimum value cause an aggregation of PCBM molecules, which reduces the ability for excitons to dissociate, consequently, causing a reduction in electronic performance. Analysis of the changes in *J–V* characteristics leads to the conclusion that thermal annealing at optimum temperature improves the performance of OPV devices. This is due to the increasing trends of both *FF* and J_{sc}, while V_{oc} remains relatively constant for all temperatures. It is shown that optimising annealing conditions requires careful consideration of the interplay between charge carrier conduction and excitonic dissociation.

Acknowledgement

This program has been supported by the Australian Government through the Australian Renewable Energy Agency (ARENA). Responsibility for the views, information or advice expressed herein is not accepted by the Australian Government. The authors would like to thank the Australian Centre for Advanced Photovoltaics, UNSW staff and technicians for their support. We are also grateful to all of our OPV group members for useful discussions and support during this work.

References

[1] Green MA, Emery K, Hishikawa Y, Warta W, Dunlop ED. Solar cell efficiency tables (version 42). Prog Photovoltaics Res Appl 2013;21:827–37.
[2] Brabec CJ. Organic photovoltaics: technology and market. Solar Energy Mater Solar Cells 2004;83:273–92.
[3] Ameri T, Khoram P, Min J, Brabec CJ. Organic ternary solar cells: a review. Adv Mater 2013;25:4245–66.
[4] Ahmad J, Bazaka K, Anderson LJ, White RD, Jacob MV. Materials and methods for encapsulation of OPV: a review. Renewable Sustainable Energy Rev 2013;27:104–17.
[5] Tang CW, VanSlyke SA. Organic electroluminescent diodes. Appl Phys Lett 1987;51:913–5.
[6] Tang CW. Two-layer organic photovoltaic cell. Appl Phys Lett 1986;48:183–5.
[7] Krebs FC, Tromholt T, Jorgensen M. Upscaling of polymer solar cell fabrication using full roll-to-roll processing. Nanoscale 2010;2:873–86.
[8] Krebs FC. Fabrication and processing of polymer solar cells: a review of printing and coating techniques. Solar Energy Mater Solar Cells 2009;93:394–412.
[9] Krebs FC, Jørgensen M, Norrman K, Hagemann O, Alstrup J, Nielsen TD, et al. A complete process for production of flexible large area polymer solar cells entirely using screen printing—first public demonstration. Solar Energy Mater Solar Cells 2009;93:422–41.
[10] Campoy-Quiles M, Ferenczi T, Agostinelli T, Etchegoin PG, Kim Y, Anthopoulos TD, et al. Morphology evolution via self-organization and lateral and vertical diffusion in polymer:fullerene solar cell blends. Nat Mater 2008;7:158–64.
[11] Wright M, Uddin A. Organic–inorganic hybrid solar cells: a comparative review. Solar Energy Mater Solar Cells 2012;107:87–111.
[12] Facchetti A. π-Conjugated polymers for organic electronics and photovoltaic cell applications. Chem Mater 2010;23:733–58.
[13] Zhokhavets U, Erb T, Gobsch G, Al-Ibrahim M, Ambacher O. Relation between absorption and crystallinity of poly(3-hexylthiophene)/fullerene films for plastic solar cells. Chem Phys Lett 2006;418:347–50.
[14] Ameri T, Li N, Brabec CJ. Highly efficient organic tandem solar cells: a follow up review. Energy Environ Sci 2013;6:2390–413.
[15] Chen HY, Hou J, Zhang S, Liang Y, Yang G, Yang Y, et al. Polymer solar cells with enhanced open-circuit voltage and efficiency. Nat Photonics 2009;3:649–53.
[16] He Z, Zhong C, Su S, Xu M, Wu H, Cao Y. Enhanced power-conversion efficiency in polymer solar cells using an inverted device structure. Nat Photonics 2012;6:593–7.
[17] Dou L, You J, Yang J, Chen CC, He Y, Murase S, et al. Tandem polymer solar cells featuring a spectrally matched low-bandgap polymer. Nat Photonics 2012;6:180–5.
[18] Guo X, Zhou N, Lou SJ, Smith J, Tice DB, Hennek JW, et al. Polymer solar cells with enhanced fill factors. Nat Photonics 2013 (advance online publication).
[19] Li W, Hendriks KH, Roelofs WSC, Kim Y, Wienk MM, RAJ. Janssen. Efficient small bandgap polymer solar cells with high fill factors for 300 nm thick films. Adv Mater 2013;25:3182–6.
[20] Rohr S. Heliatek consolidates its technology leadership by establishing a new world record for organic solar technology with a cell efficiency of 12% 2013. http://www.heliatek.com.
[21] Krebs FC, Nielsen TD, Fyenbo J, Wadstrom M, Pedersen MS. Manufacture, integration and demonstration of polymer solar cells in a lamp for the Lighting Africa initiative. Energy Environ Sci 2010;3:512–25.
[22] Krebs FC, Fyenbo J, Tanenbaum DM, Gevorgyan SA, Andriessen R, van Remoortere B, et al. The OE-A OPV demonstrator anno domini 2011. Energy Environ Sci 2011;4:4116–23.
[23] Espinosa N, Lenzmann FO, Ryley S, Angmo D, Hosel M, Sondergaard RR, et al. OPV for mobile applications: an evaluation of roll-to-roll processed indium and silver free polymer solar cells through analysis of life cycle, cost and layer quality using inline optical and functional inspection tools. J Mater Chem A 2013;1:7037–49.
[24] Sariciftci NS, Smilowitz L, Heeger AJ, Wudl F. Photoinduced electron transfer from a conducting polymer to buckminsterfullerene. Science 1992;258:1474–6.
[25] Yu G, Gao J, Hummelen JC, Wudl F, Heeger AJ. Polymer photovoltaic cells: enhanced efficiencies via a network of internal donor–acceptor heterojunctions. Science 1995;270:1789–91.
[26] Hummelen JC, Knight BW, LePeq F, Wudl F, Yao J, Wilkins CL. Preparation and characterization of fulleroid and methanofullerene derivatives. J Org Chem 1995;60:532–8.

[27] Brabec CJ, Shaheen SE, Winder C, Sariciftci NS, Denk P. Effect of LiF/metal electrodes on the performance of plastic solar cells. Appl Phys Lett 2002;80:1288–90.
[28] Wienk MM, Kroon JM, Verhees WJH, Knol J, Hummelen JC, van Hal PA, et al. Efficient methano[70]fullerene/MDMO-PPV bulk heterojunction photovoltaic cells. Angew Chem Int Ed 2003;42:3371–5.
[29] Mihailetchi VD, Xie HX, de Boer B, LJA Koster, PWM. Blom. Charge transport and photocurrent generation in poly(3-hexylthiophene): methanofullerene bulk-heterojunction solar cells. Adv Funct Mater 2006;16:699–708.
[30] Yang X, Loos J, Veenstra SC, Verhees WJH, Wienk MM, Kroon JM, et al. Nanoscale morphology of high-performance polymer solar cells. Nano Lett 2005;5:579–83.
[31] Ryu MS, Cha HJ, Jang J. Effects of thermal annealing of polymer:fullerene photovoltaic solar cells for high efficiency. Curr Appl Phys 2010;10:S206–9.
[32] Moulé AJ, Meerholz K. Controlling morphology in polymer–fullerene mixtures. Adv Mater 2008;20:240–5.
[33] Kim K, Liu J, Namboothiry MAG, Carroll DL. Roles of donor and acceptor nanodomains in 6% efficient thermally annealed polymer photovoltaics. Appl Phys Lett 2007;90:163511–3.
[34] Park SH, Roy A, Beaupre S, Cho S, Coates N, Moon JS, et al. Bulk heterojunction solar cells with internal quantum efficiency approaching 100%. Nat Photonics 2009;3:297–302.
[35] Brabec CJ, Gowrisanker S, Halls JJM, Laird D, Jia S, Williams SP. Polymer–fullerene bulk-heterojunction solar cells. Adv Mater 2010;22:3839–56.
[36] Bull TA, Pingree LSC, Jenekhe SA, Ginger DS, Luscombe CK. The role of mesoscopic PCBM crystallites in solvent vapor annealed copolymer solar cells. ACS Nano 2009;3:627–36.
[37] Chen F-C, Ko C-J, Wu J-L, Chen W-C. Morphological study of P3HT:PCBM blend films prepared through solvent annealing for solar cell applications. Solar Energy Mater Solar Cells 2010;94:2426–30.
[38] Kim Y, Ballantyne AM, Nelson J, Bradley DDC. Effects of thickness and thermal annealing of the PEDOT:PSS layer on the performance of polymer solar cells. Org Electron 2009;10:205–9.
[39] Zeng L, Tang CW, Chen SH. Effects of active layer thickness and thermal annealing on polythiophene: fullerene bulk heterojunction photovoltaic devices. Appl Phys Lett 2010;97:053305 (3).
[40] Schilinsky P, Asawapirom U, Scherf U, Biele M, Brabec CJ. Influence of the molecular weight of poly(3-hexylthiophene) on the performance of bulk heterojunction solar cells. Chem Mater 2005;17:2175–80.
[41] Ka ukauskas V, Arlauskas A, Pranaitis M, Glatthaar M, Hinsch A. Charge transport and trapping in bulk-heterojunction solar cells. J Nanosci Nanotechnol 2010;10:1376–80.
[42] Chang L, Lademann HWA, Bonekamp JB, Meerholz K, Moulé AJ. Effect of trace solvent on the morphology of P3HT:PCBM bulk heterojunction solar cells. Adv Funct Mater 2011;21:1779–87.
[43] Kim JS, Lee JH, Park JH, Shim C, Sim M, Cho K. High-efficiency organic solar cells based on preformed poly(3-hexylthiophene) nanowires. Adv Funct Mater 2011;21:480–6.
[44] Kim MH, Sun M, Gowrishankar V, McGehee MD, Kwon YU. Confinement effects of P3HT in nanochannels and their implications for bulk heterojunction solar cells. J Nanosci Nanotechnol 2010;10:279–84.
[45] Krishnamoorthy T, Thavasi V, Subodh G M, Ramakrishna S. A first report on the fabrication of vertically aligned anatase TiO_2 nanowires by electrospinning: preferred architecture for nanostructured solar cells. Energy Environ Sci 2011;4:2807–12.
[46] Mor GK, Shankar K, Paulose M, Varghese OK, Grimes CA. High efficiency double heterojunction polymer photovoltaic cells using highly ordered TiO_2 nanotube arrays. Appl Phys Lett 2007;91:152111–3.
[47] Yin B, Liu Q, Yang L, Wu X, Liu Z, Hua Y, et al. Buffer layer of PEDOT:PSS/graphene composite for polymer solar cells. J Nanosci Nanotechnol 2010;10:1934–8.
[48] Motaung DE, Malgas GF, Arendse CJ, Mavundla SE, Oliphant CJ, Knoesen D. Thermal-induced changes on the properties of spin-coated P3HT:C_{60} thin films for solar cell applications. Solar Energy Mater Solar Cells 2009;93:1674–80.
[49] Cai W, Gong X, Cao Y. Polymer solar cells: recent development and possible routes for improvement in the performance. Solar Energy Mater Solar Cells 2010;94:114–27.
[50] Chirvase D, Parisi J, Hummelen JC, Dyakonov V. Influence of nanomorphology on the photovoltaic action of polymer–fullerene composites. Nanotechnology 2004;15:1317–23.
[51] Kim Y, Choulis SA, Nelson J, Bradley DDC, Cook S, Durrant JR. Device annealing effect in organic solar cells with blends of regioregular poly(3-hexylthiophene) and soluble fullerene. Appl Phys Lett 2005;86:063502–3.
[52] Li G, Shrotriya V, Huang J, Yao Y, Moriarty T, Emery K, et al. High-efficiency solution processable polymer photovoltaic cells by self-organization of polymer blends. Nat Mater 2005;4:864–8.
[53] Kim Y, Cook S, Tuladhar SM, Choulis SA, Nelson J, Durrant JR, et al. A strong regioregularity effect in self-organizing conjugated polymer films and high-efficiency polythiophene:fullerene solar cells. Nat Mater 2006;5:197–203.
[54] Erb T, Zhokhavets U, Gobsch G, Raleva S, Stühn B, Schilinsky P, et al. Correlation between structural and optical properties of composite polymer/fullerene films for organic solar cells. Adv Funct Mater 2005;15:1193–6.
[55] Saunders BR. Hybrid polymer/nanoparticle solar cells: preparation, principles and challenges. J Colloid Interface Sci 2012;369:1–15.
[56] Garcia-Belmonte G, Munar A, Barea EM, Bisquert J, Ugarte I, Pacios R. Charge carrier mobility and lifetime of organic bulk heterojunctions analyzed by impedance spectroscopy. Org Electron 2008;9:847–51.
[57] Bundgaard E, Krebs FC. Low band gap polymers for organic photovoltaics. Solar Energy Mater Solar Cells 2007;91:954–85.
[58] Bundgaard E, Shaheen SE, Krebs FC, Ginley DS. Bulk heterojunctions based on a low band gap copolymer of thiophene and benzothiadiazole. Solar Energy Mater Solar Cells 2007;91:1631–7.
[59] Hou J, Chen HY, Zhang S, Chen RI, Yang Y, Wu Y, et al. Synthesis of a low band gap polymer and its application in highly efficient polymer solar cells. J Am Chem Soc 2009;131:15586–7.
[60] Hou J, Chen HY, Zhang S, Li G, Yang Y. Synthesis, characterization, and photovoltaic properties of a low band gap polymer based on silole-containing polythiophenes and 2,1,3-benzothiadiazole. J Am Chem Soc 2008;130:16144–5.
[61] Hou J, Chen TL, Zhang S, Chen HY, Yang Y. Poly[4,4-bis(2-ethylhexyl) cyclopenta[2,1-b;3,4-b']dithiophene-2, 6-diyl-alt-2,1,3-benzoselenadiazole-4,7-diyl], a new low band gap polymer in polymer solar cells. J Phys Chem C 2009;113:1601–5.
[62] Gregg BA, Hanna MC. Comparing organic to inorganic photovoltaic cells: theory, experiment, and simulation. J Appl Phys 2003;93:3605–14.
[63] Zuo L, Jiang X, Xu M, Yang L, Nan Y, Yan Q, et al. Enhancement of short current density in polymer solar cells with phthalocyanine tin (IV) dichloride as interfacial layer. Solar Energy Mater Solar Cells 2011;95:2664–9.
[64] Yip H-L, Jen AKY. Recent advances in solution-processed interfacial materials for efficient and stable polymer solar cells. Energy Environ Sci 2012;5:5994–6011.
[65] Brabec CJ, Cravino A, Meissner D, Serdar Sariciftci N, Fromherz T, Rispens MT, et al. Origin of the open circuit voltage of plastic solar cells. Adv Funct Mater 2001;11:374–80.
[66] Scharber MC, Mühlbacher D, Koppe M, Denk P, Waldauf C, Heeger AJ, et al. Design rules for donors in bulk-heterojunction solar cells—towards 10% energy-conversion efficiency. Adv Mater 2006;18:789–94.
[67] Yamanari T, Taima T, Sakai J, Saito K. Origin of the open-circuit voltage of organic thin-film solar cells based on conjugated polymers. Solar Energy Mater Solar Cells 2009;93:759–61.
[68] Potscavage Jr WJ, Sharma A, Kippelen B. Critical interfaces in organic solar cells and their influence on the open-circuit voltage. Acc Chem Res 2009;42:1758–67.
[69] Green MA, Emery K, Hishikawa Y, Warta W, Dunlop ED. Solar cell efficiency tables (version 39). Prog Photovoltaics Res Appl 2012;20:12–20.
[70] Zhao J, Wang A, Green MA. 24.5% efficiency silicon PERT cells on MCZ substrates and 24.7% efficiency PERL cells on FZ substrates. Prog Photovoltaics Res Appl 1999;7:471–4.
[71] Gupta D, Mukhopadhyay S, Narayan KS. Fill factor in organic solar cells. Solar Energy Mater Solar Cells 2010;94:1309–13.
[72] Kirchartz T, Taretto K, Rau U. Efficiency limits of organic bulk heterojunction solar cells. J Phys Chem C 2009;113:17958–66.
[73] Servaites JD, Ratner MA, Marks TJ. Practical efficiency limits in organic photovoltaic cells: functional dependence of fill factor and external quantum efficiency. Appl Phys Lett 2009;95:163302–3.
[74] Yablonovitch E. Statistical ray optics. J Opt Soc Am 1982;72:899–907.
[75] Dennler G, Scharber MC, Brabec CJ. Polymer–fullerene bulk-heterojunction solar cells. Adv Mater 2009;21:1323–38.
[76] Bavel SSv Sourty E, Gd With, Loos J. Three-dimensional nanoscale organization of bulk heterojunction polymer solar cells. Nano Lett 2008;9:507–13.
[77] Ma W, Yang C, Gong X, Lee K, Heeger AJ. Thermally stable, efficient polymer solar cells with nanoscale control of the interpenetrating network morphology. Adv Funct Mater 2005;15:1617–22.
[78] Guo T-F, Wen T-C, L'Vovich Pakhomov G, Chin X-G, Liou S-H, Yeh P-H, et al. Effects of film treatment on the performance of poly(3-hexylthiophene)/soluble fullerene-based organic solar cells. Thin Solid Films 2008;516:3138–42.
[79] Agostinelli T, Lilliu S, Labram JG, Campoy-Quiles M, Hampton M, Pires E, et al. Real-time investigation of crystallization and phase-segregation dynamics in P3HT:PCBM solar cells during thermal annealing. Adv Funct Mater 2011;21:1701–8.
[80] Dante M, Peet J, Nguyen TQ. Nanoscale charge transport and internal structure of bulk heterojunction conjugated polymer/fullerene solar cells by scanning probe microscopy. J Phys Chem C 2008;112:7241–9.
[81] Reyes-Reyes M, Kim K, Carroll DL. High-efficiency photovoltaic devices based on annealed poly(3-hexylthiophene) and 1-(3-methoxycarbonyl)-propyl-1-phenyl-(6,6)C_{61} blends. Appl Phys Lett 2005;87:083506 (3).
[82] Wang W, Wu H, Yang C, Luo C, Zhang Y, Chen J, et al. High-efficiency polymer photovoltaic devices from regioregular-poly(3-hexylthiophene-2,5-diyl) and [6,6]-phenyl-C_{61}-butyric acid methyl ester processed with oleic acid surfactant. Appl Phys Lett 2007;90:183512–3.
[83] Wang T, Pearson AJ, Lidzey DG, RAL. Jones. Evolution of structure, optoelectronic properties, and device performance of polythiophene:fullerene solar cells during thermal annealing. Adv Funct Mater 2011;21:1383–90.
[84] Kim JY, Noh S, Kwak J, Lee C. Analysis of annealing process on P3HT:PCBM-based polymer solar cells using optical and impedance spectroscopy. J Nanosci Nanotechnol 2013;13:3360–4.
[85] Pearson AJ, Wang T, Jones RAL, Lidzey DG, Staniec PA, Hopkinson PE, et al. Rationalizing phase transitions with thermal annealing temperatures for P3HT: PCBM organic photovoltaic devices. Macromolecules 2012;45:1499–508.
[86] Kim H, Shin M, Kim Y. Distinct annealing temperature in polymer:fullerene: polymer ternary blend solar cells. J Phys Chem C 2009;113:1620–3.
[87] Kim S-O, Sung Chung D, Cha H, Wan Jang J, Kim Y-H, Kang J-W, et al. Thermally stable organic bulk heterojunction photovoltaic cells incorporating an amorphous fullerene derivative as an electron acceptor. Solar Energy Mater Solar Cells 2011;95:432–9.

[88] Kim H, So W-W, Moon S-J. The importance of post-annealing process in the device performance of poly(3-hexylthiophene): methanofullerene polymer solar cell. Solar Energy Mater Solar Cells 2007;91:581–7.
[89] Zhang C, Tong SW, Zhu C, Jiang C, Kang ET, Chan DSH. Enhancement in open circuit voltage induced by deep interface hole traps in polymer–fullerene bulk heterojunction solar cells. Appl Phys Lett 2009;94:103305 (3).
[90] Oklobia O, Shafai TS. A quantitative study of the formation of PCBM clusters upon thermal annealing of P3HT/PCBM bulk heterojunction solar cell. Solar Energy Mater Solar Cells 2013;117:1–8.
[91] Padinger F, Rittberger RS, Sariciftci NS. Effects of postproduction treatment on plastic solar cells. Adv Funct Mater 2003;13:85–8.
[92] Oklobia O, Shafai TS. A study of donor/acceptor interfaces in a blend of P3HT/PCBM solar cell: effects of annealing and PCBM loading on optical and electrical properties. Solid-State Electron 2013;87:64–8.
[93] Kong H, Moon JS, Cho NS, Jung IH, Park M-J, Park J-H, et al. Thermal annealing induced bicontinuous networks in bulk heterojunction solar cells and bipolar field-effect transistors. Appl Phys Lett 2009;95:173301–3.
[94] Jørgensen M, Norrman K, Gevorgyan SA, Tromholt T, Andreasen B, Krebs FC. Stability of polymer solar cells. Adv Mater 2012;24:580–612.
[95] Bertho S, Haeldermans I, Swinnen A, Moons W, Martens T, Lutsen L, et al. Influence of thermal ageing on the stability of polymer bulk heterojunction solar cells. Solar Energy Mater Solar Cells 2007;91:385–9.
[96] Norrman K, Madsen MV, Gevorgyan SA, Krebs FC. Degradation patterns in water and oxygen of an inverted polymer solar cell. J Am Chem Soc 2010;132:16883–92.
[97] Schumann S, Da Campo R, Illy B, Cruickshank AC, McLachlan MA, Ryan MP, et al. Inverted organic photovoltaic devices with high efficiency and stability based on metal oxide charge extraction layers. J Mater Chem 2011;21:2381–6.
[98] Søndergaard R, Hösel M, Angmo D, Larsen-Olsen TT, Krebs FC. Roll-to-roll fabrication of polymer solar cells. Mater Today 2012;15:36–49.
[99] Krebs FC. Roll-to-roll fabrication of monolithic large-area polymer solar cells free from indium-tin-oxide. Solar Energy Mater Solar Cells 2009;93:1636–41.
[100] Søndergaard RR, Hösel M, Krebs FC. Roll-to-Roll fabrication of large area functional organic materials. J Polym Sci Part B: Polym Phys 2013;51:16–34.
[101] Li G, Zhu R, Yang Y. Polymer solar cells. Nat Photonics 2012;6:153–61.